ACS APPLIED MATERIALS & INTERFACES

Research Article

www.acsami.org

Enhancement in Ion Adsorption Rate and Desalination Efficiency in a Capacitive Deionization Cell through Improved Electric Field Distribution Using Electrodes Composed of Activated Carbon Cloth Coated with Zinc Oxide Nanorods

Karthik Laxman,[†,‡] Myo Tay Zar Myint,[†] Hadj Bourdoucen,[‡,§] and Joydeep Dutta*[,†]

[†]Chair in Nanotechnology, Water Research Center, Sultan Qaboos University, PO Box 33, Al-Khoudh, Muscat−123, Sultanate of Oman

[‡]Department of Electrical and Computer Engineering, College of Engineering, Sultan Qaboos University, Al-Khoudh, Muscat−123, Sultanate of Oman

[§]Communication and Information Research Center (CIRC), Sultan Qaboos University, Al-Khoudh, Muscat−123, Sultanate of Oman

Supporting Information

ABSTRACT: Electrodes composed of activated carbon cloth (ACC) coated with zinc oxide (ZnO) nanorods are compared with plain ACC electrodes, with respect to their desalination efficiency of a 17 mM NaCl solution at different applied potentials. Polarization of the ZnO nanorods increased the penetration depth and strength of the electric field between the electrodes, leading to an increase in the capacitance and charge efficiency at reduced input charge ratios. Uniform distribution of the electric field lines between two electrodes coated with ZnO nanorods led to faster ion adsorption rates, reduced the electrode saturation time, and increased the average desalination efficiency by ∼45% for all applied potentials. The electrodes were characterized for active surface area, capacitance from cyclic voltammetry, theoretical assessment of surface area utilization, and the magnitude of electric field force acting on an ion of unit charge for each potential.

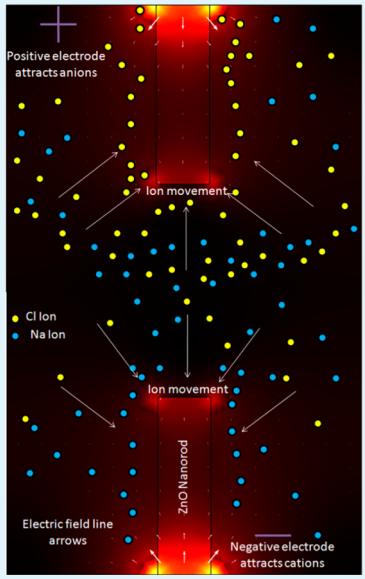

KEYWORDS: *electric field, capacitive deionization, zinc oxide, activated carbon cloth, charge efficiency*

1. INTRODUCTION

Desalted water is becoming an important source of domestic water supplement in many countries.[1] With a wide variation of salt content in the available water sources, traditional desalting technologies involving multistage flash (MSF) and reverse osmosis (RO) may prove uneconomical, especially for low salinity and remote water sources. Capacitive deionization with lower installation costs and lower energy requirements is an alternative for desalting low salinity water.[2,3] Capacitive deionization (CDI) cells work on the principle of potential-dependent electric-field-mediated ion adsorption in the electrical double layer (EDL) formed at the electrode surface.[4−6] The most commonly used electrode materials for CDI are carbon-based, because of its inertness, high surface area, and low fabrication costs.[7] Electrically conducting activated carbon cloths, which have a high surface area, are easy to handle and are ideal for application as electrodes in CDI.[8,9]

By convention, an electric field consists of lines of force extending from the positive electrode to the negative electrode, attracting and repelling anions and cations, respectively. Electric field strength is directly proportional the potential applied between the electrodes and can assist in increasing ion adsorption with a tradeoff in the power requirements. Analogous to a capacitor, the charge stored on the electrode surface can be enhanced by coating the electrode with a dielectric material to enhance charge storage and reduce the leakage current and power consumption.[10,11]

Received: February 19, 2014
Accepted: June 18, 2014
Published: June 18, 2014

Previous studies have shown that, by coating an activated carbon cloth (ACC) surface with titania (TiO_2) nanoparticles, the electrosorption capacity of the electrode increased, partly due to localized electric field enhancement at the surface of the nanoparticles.[9,12] Zinc oxide (ZnO) has a bandgap similar to that of TiO_2,[13] and its wurtzite crystal structure leads to a preferential growth of nanorods in the vertical *c*-axis[14,15] on a wide array of surfaces.[16−18] It has also shown promise as a material for uniformly distributed field emission along its surface.[19−21] ZnO nanorods grown on ACC can potentially mask a fraction of the micropores and mesopores, which is redundant in the short time scales used for deionization, while the exposed nanorods surfaces provide easy access to ion adsorption, effectively increasing the active surface area for electrosorption.[22]

In this paper, we report an increase in the desalination efficiency attributed to enhanced electric field distribution after growing ZnO nanorods on the ACC surface of symmetric CDI electrodes. The nanorods-coated ACC electrode was characterized for power consumption, charge efficiency, and electric field enhancement, which is reported here.

2. RESULTS AND DISCUSSION

In capacitive deionization (CDI), a typical desalination cycle consists of accumulation of anions/cations in the electrical double layer (EDL), the thickness of which is dependent on the applied electric field between the two conducting electrodes. The resulting force from electric field acting from the positive electrode to the negative electrode (circuit ground) is expressed as the force experienced by a unit positive charge placed in the electric field (in our case, the Na^+ ion). Thus, the removal of Na^+ from solution is a combination of both attraction by the negative electrode and repulsion by the positive electrodes. Cl^- ions would follow the opposing cycle. Figure 1a shows the effect of increasing the applied potential on the desalination efficiency of a CDI device using symmetric activated carbon cloth (ACC) electrodes. A relatively linear adsorption and desorption of ions are observed both during the desalination and the regeneration cycles, which is consistently repeatable (see Figure S4 in the Supporting Information). With an increase in the applied potential, the field strength, which can be expressed as a ratio of the applied potential to the distance between the electrodes (eq 1), increases.

$$E = \frac{V}{d} \tag{1}$$

where V is the applied potential (in volts, V) and d is the mean distance (due to the nonhomogeneous electrode surface) between the electrodes (expressed in meters, m).

The increased field strength leads to an increase in the force available for ion adsorption, leading to an increase in the ion uptake of the micropores, mesopores, and macropores in ACC.[23]

Electric field can also be expressed by Coulomb's law as

$$E = \frac{F}{q} \tag{2}$$

where E is the electric field (in volts per meter, V/m), F the force (in newtons, N), and q the charge on the particles (in coulombs, C).

Considering point charges distributed on the ACC surface, the electric force between two charges q (the charge on the ion) and Q (the total charge on ACC surface during a deionization cycle) separated by a distance d between them, is given by

$$F = \frac{KqQ}{d^2} \tag{3}$$

where K is a constant of proportionality ($K = 9.0 \times 10^9$ N m^2/C).

Thus, by calculating the total charge delivered to the ACC surface, we can estimate the attraction/repulsion force acting on an ion of unit charge in the space between the electrodes. The total charge for a single deionization cycle is extracted by integrating the area under the charging current curve between the limits of charging time. Figure 1b shows a plot of the resultant force acting on an ionic charge at the counter electrode for an applied potential and the efficiency of desalination, which suggests that ion adsorption on the ACC electrode is weakly proportional to the attraction/repulsion force between the electrodes. As the applied voltage increases, the force, which is a function of the charge on the electrodes, decreases (at 2.0 V), which we attribute to the hydrolysis of water. A simultaneous increase in the current rating suggests an increase in leakage current between the electrodes, leading to

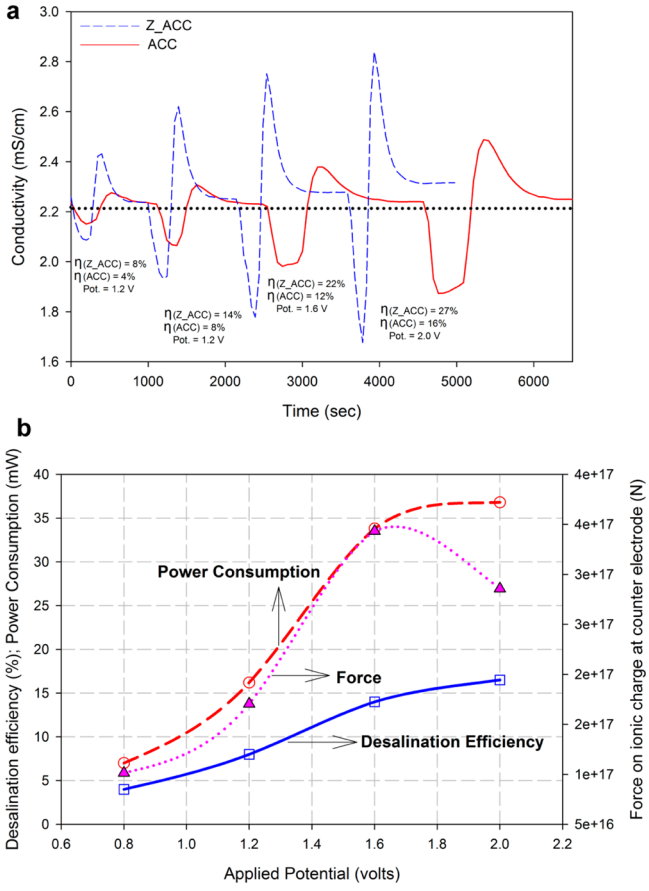

Figure 1. (a) Conductivity change during adsorption and desorption on ACC and ACC electrodes coated with ZnO nanorods for variable applied potentials and a feed solution of 1000 ppm of NaCl. The flow rate for the system was maintained at 3 mL/min. The weight of the electrodes was kept constant at 0.275 g. (b) Desalination efficiency as a function of the electrical field force and power consumption on ACC electrodes.

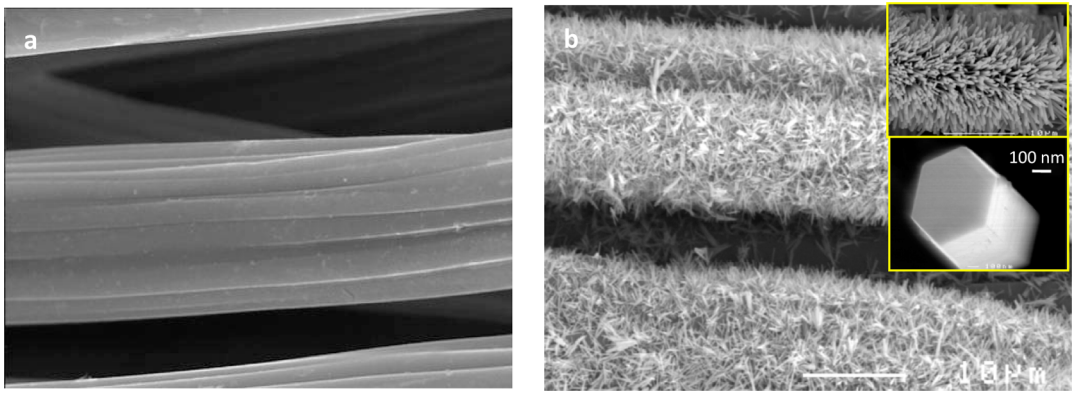

Figure 2. Field-emission scanning electron microscopy (FESEM) images of (a) ACC surface without any coating and (b) ACC coated with ZnO nanorods, showing nanorods with an average length of ~8 μm and a dense coverage. (Insets in panel b show magnified views of the ZnO nanorods, showing the hexagonal structure of the rods.)

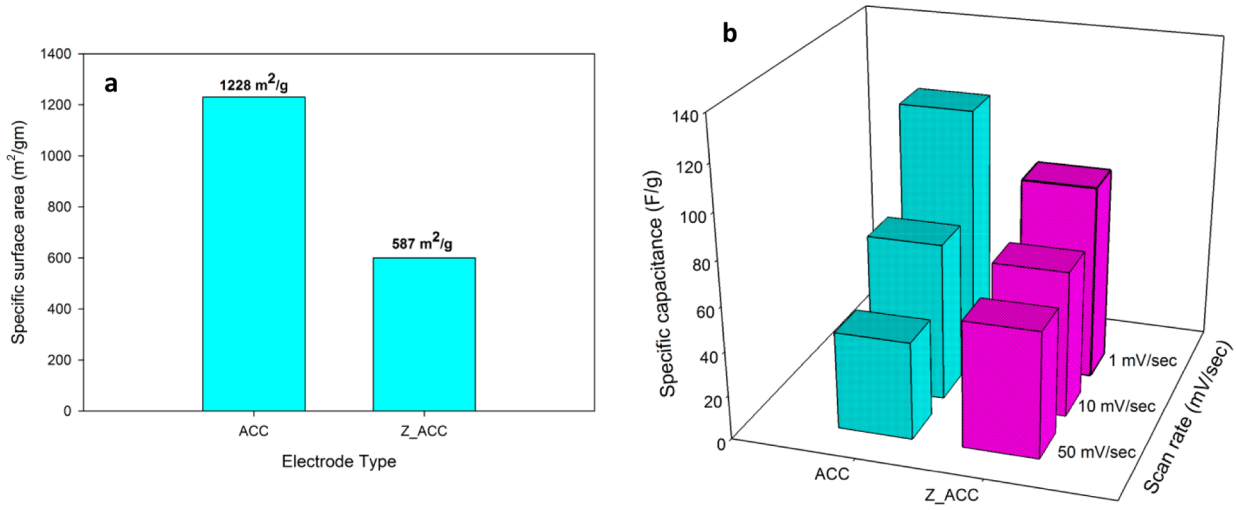

Figure 3. Comparison of ACC and ACC coated with ZnO nanorods (Z_ACC), with respect to (a) active surface area from NMR measurements and (b) capacitance, which was calculated from the cyclic voltammetry curves (see section III in the Supporting Information).

an increase in the power consumption of the cell at the high potential.

Upon the addition of a layer of ZnO nanorods on the ACC surface, the desalination efficiency was found to increase by an average of 45% for all applied potentials with a considerable reduction in the charging time (Figure 1a), suggesting faster adsorption dynamics at the electrode surface. There was also a noticeable increase in the equilibrium conductivity of the regenerated solution, which is attributed to the longer time required for a solution to reach its original conductivity and is being further investigated. Dissolution of ZnO in the solution was ruled out, based on ICP measurements, which showed negligible Zn ions in desalinated and regenerated solutions (results not reported here).

The as-grown nanorods are 7−9 μm in length, with an average diameter of ~500 nm and a hexagonal wurtzite crystal structure (see Figure 2 and Figure S2 in the Supporting Information) that is composed of a zinc-rich polar plane (0001), together with mixed terminated planes (0110, 1010, 1100), which are relatively nonpolar in nature.[24]

Upon the addition of ZnO nanorods on the ACC surface, the electrode surface area was found to decrease from ~1230 m^2/g to 587 m^2/g (see Figure 3a). In contrast, capacitance measurements extracted from the area under the current curve of the CV graphs (see Figure S3 in the Supporting Information) suggest that, at lower scan rates (1 mV/s), the surface of ACC coated with ZnO nanorods (henceforth referred to as Z_ACC) has lower capacitance, compared to ACC; however, upon increasing the scan rate to 50 mV/s, Z_ACC showed higher charge storage capacity (see Figure 3b).

Although surface area and capacitance are generally proportional, it is possible that the nanometric dimensions between the rods with the exposed mixed terminated planes, having a relatively nonpolar nature, might prevent the penetration of water (due to high surface tension of water), which could explain the reduced surface area estimated from NMR measurements. This was confirmed when the surface area of the Z_ACC electrode increased from ~600 m^2/g to 760 m^2/g upon changing the solvent to ethanol, which has a lower surface tension (see Table S1 in the Supporting Information). However, the surface area was still less than that of ACC. Thus, it is possible that, at higher scan rates, a majority of the micropores in ACC cannot be accessed by the ions due to the short time span for adsorption. Overlapping double layers at the micropore entrance can block incoming ions, further reducing the capacitance.[6] On the other hand, well-distributed voltage-mediated electric field lines that extend along the nanorod surfaces[25] can increase the charge and energy on the

crystal planes,[26] making them hydrophilic and increasing their affinity for ion adsorption. This, combined with the well-exposed nanorod surfaces reduces the barrier for ion adsorption and is possibly the reason for higher capacitance ratings at the higher scan rates. This phenomenon is especially important for CDI systems, where the applied potential is generally a step function with a steep rise time.

The charging currents of the ACC and Z_ACC electrodes further confirmed the capacitance measurements (see Figure 4a). The initial peak inrush current (I) for any capacitor is given by

$$I = \frac{\mathrm{d}Q(t)}{\mathrm{d}t} = C\frac{\mathrm{d}V(t)}{\mathrm{d}t} \tag{4}$$

where C is the capacitance, $V(t)$ the potential applied across the capacitor, and $Q(t)$ the rate of change of charge on the capacitor.

With a constant rate of change in the applied potential, a higher peak inrush charging current for Z_ACC (Figure 4a) indicates higher capacitance, compared to ACC electrodes, followed by a fast decay, suggesting faster ion adsorption. The charging current curves for ACC and Z_ACC (at 1.6 V) were fitted with a second-order exponential equation (eq 5) for analyzing the rate of ion adsorption and power consumption per desalination cycle:

$$Y = a\exp(-bx) + c\exp(dx) \tag{5}$$

The ion adsorption rate was extracted from the charging current curve by taking a first-order differential of the fitting function, to yield a plot of the rate of ion adsorption for both ACC and Z_ACC electrodes at an applied potential of 1.6 V (Figure 4b). A substantial increase in the potency of the Z_ACC electrode for fast ion adsorption can be observed, leading to faster surface saturation which explains the reduction in the deionization time.

Considering that the weights of all electrodes were kept constant at 0.275 g and that the total surface area was decreased upon coating with ZnO nanorods, the enhancement in ion adsorption efficiency and rate suggests that enhanced field strength due to stored charges on the ZnO surface could be the primary driving force mediating the improved adsorption.

To characterize the cut-in potential at which a ZnO nanorod surface can be charged to develop an electric field, we measured the $I-V$ characteristics of the ZnO nanorods (Figure 5a) from the tip to the base. The $I-V$ plot shows that ZnO is easily polarizable and can generate current in the mA range at potentials below 1.0 V, making it a suitable material for enhancing the electric field strength at the electrode. The

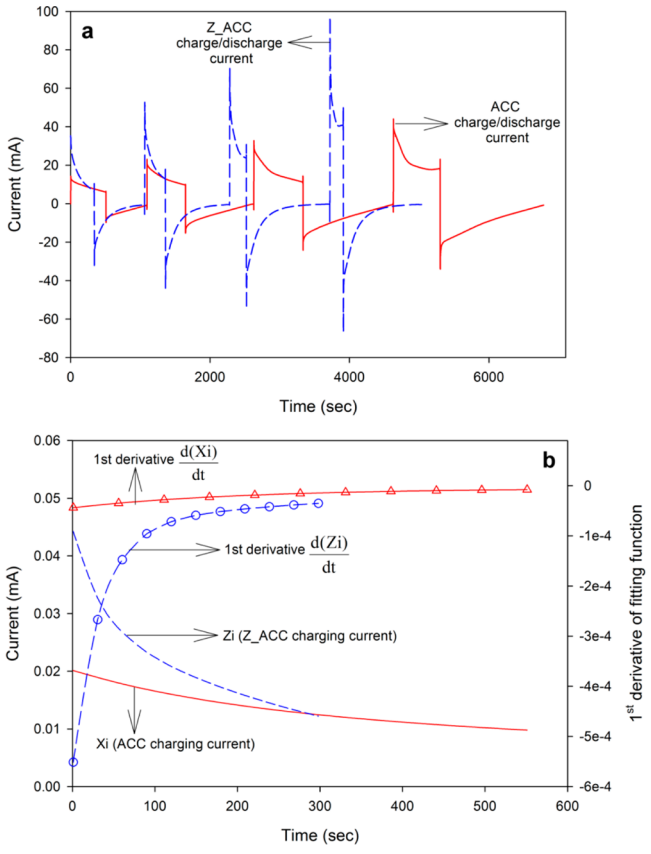

Figure 4. (a) Charging and discharging currents for ACC and Z_ACC electrodes for variable applied potential during the deionization process of a 1000 ppm of NaCl solution at a flow rate of 2 mL/min. (b) First-order differential of the charging current (at an applied potential of 1.2 V) for ACC and Z_ACC electrodes, showing an increased rate of ion adsorption and faster surface saturation for the Z_ACC electrode.

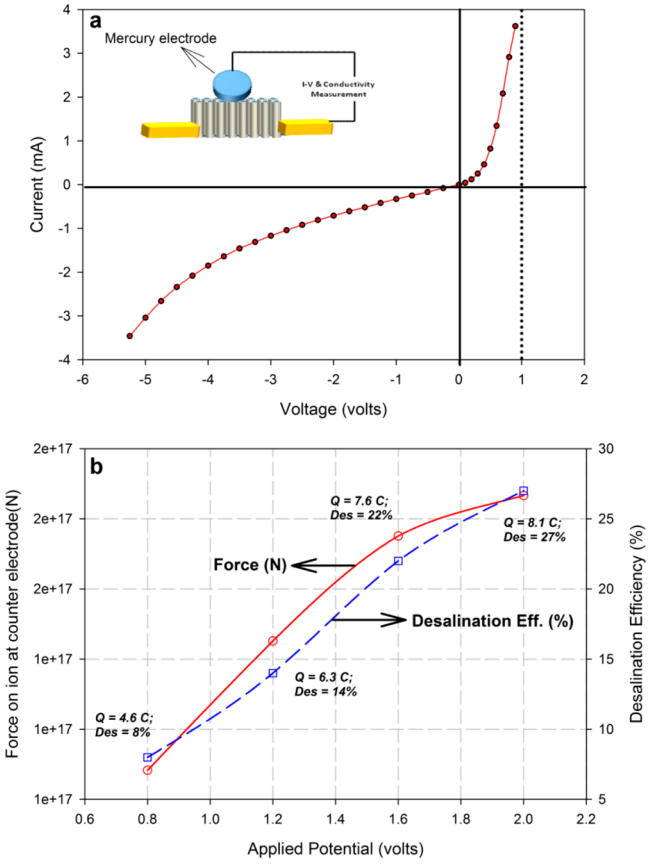

Figure 5. (a) Current–voltage ($I-V$) characteristics of ZnO nanorods measured from the tip to the base of the rod using a drop of mercury as one electrode and gold-plated glass as the second electrode. (b) Desalination efficiency of Z_ACC electrodes for variable applied potentials and the force for ion attraction at the counter electrode, with respect to the applied potential.

reduced rate of current rise in the negative voltage region could be due to the Schottky junction formed at the gold−ZnO junction,[27] where energy must be supplied to overcome the barrier height θ_{SB}, given by

$$\theta_{SB} = \theta_M - \chi_S \quad (6)$$

where θ_M is the work function of metal and χ_s is the electron affinity of ZnO.

As evident in the graph (Figure 5a), at an applied voltage of 1.0 V, the applied field is ~2×10^{-4} V/μm (electrode spacing of 5 mm), which is above the threshold for surface charge accumulation. For the CDI cell, with an electrode spacing of 650 μm and an applied potential of 1.6 V, the resulting field between the electrodes is 2.45×10^{-3} V/μm, which is well above the ZnO threshold (as seen in Figure 5a) and can lead to the generation of a strong electric field all along the surface of the nanorods. The applied field is also orders of magnitude below the threshold for field emission,[25] which will minimize water hydrolysis and unwanted redox reactions at the electrode surface. A plot of the resultant electric force per charge (N/C), with respect to the applied field for Z_ACC electrode, is shown in Figure 5b. The total charge delivered to the Z_ACC electrode was extracted by integrating the charging current fitting function (eq 7) to give the total charge delivered to the electrode surface for a single deionization cycle. From the figure, we can see that the charge-dependent electric field and desalination efficiency are almost linear in nature in the case of Z_ACC electrodes.

$$\int_{x=0}^{x=t} Y = a \exp(-bx) + c \exp(dx) \rightarrow Q_t \quad (7)$$

where $x = 0$ and $x = t$ are the limits of the charging time and Q_t is the total stored charge on the electrode surface for a particular charge (deionization) cycle.

It is interesting to note that the amount of charge delivered to the Z_ACC surface at higher potentials is considerably lower than the charge delivered to the ACC electrode surface (Figure 6a). This is attributed to the dielectric nature of ZnO storing charges within the material, which leads to faster ion adsorption rates. This leads to a reduction in the time required for Z_ACC surface saturation and, hence, the total charge or energy consumption for the desalination process. Charge efficiencies calculated from the ratio of charge adsorbed from solution to charge delivered to the electrode (current), showed that Z_ACC electrodes perform better at all potentials except at 2.0 V (Figure 6b). A tradeoff between the energy utilized and desalination achieved is always present and it would be best to work at potentials below 2.0 V for optimized performance. A more-tangible comparison between the electrodes is the moles of salt adsorbed per gram of electrode per second (mol/g/s), where the superiority of Z_ACC is clearly established (Figure 6b). In fact, a straightforward calculation of the mass of salt adsorbed per unit mass of electrode material (mg/g, calculated at an optimized potential of 1.6 V) shows that Z_ACC electrodes can adsorb almost double the salt, compared to ACC electrodes, and is comparable with the present literature (see Table 1).[28]

The total power required to obtain 1 m^3 of desalinated water (at 1.6 V) for Z-ACC electrodes was calculated to be ~0.5 kWh, while for each desalination cycle, the power consumed is 23.5 mW, both of which are below the standard power requirements of today.[2,28,29] Further optimization of the electrode and cell structure helped us to achieve a considerable increase in desalination efficiency for both high- and low-concentration NaCl solutions at an applied potential of 1.6 V, as shown in Table 2.

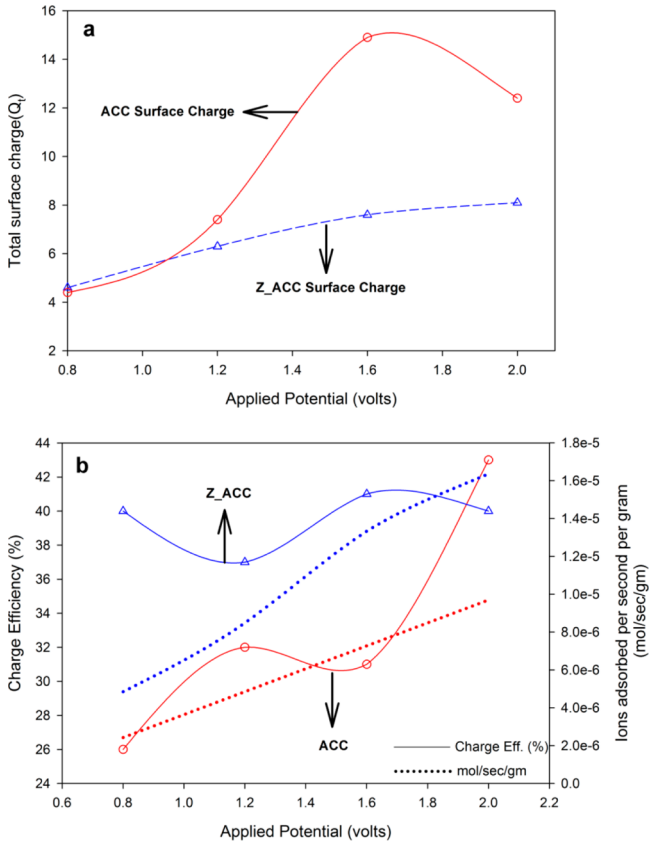

Figure 6. (a) Total charge stored on the ACC and Z_ACC electrode surfaces (in coulombs) for the duration of the charging time at a given potential. (b) Comparison of the ACC electrodes (red traces) and Z_ACC electrodes (blue traces), with respect to charge efficiency (full lines) and ions adsorbed per second per gram of electrode (dotted lines), showing that power consumption is optimized at potentials below 2.0 V.

Table 1. Table Showing the Salt Uptake of the ACC Electrodes and ACC Electrodes Coated with ZnO Nanorods (in mg/g per Desalination Cycle) at an Applied Potential of 1.6 V DC for a 17 mM NaCl Feed Solution

material	mg of salt/g of electrode at 1.6 V
ACC	1.92 mg/g
ZnO ACC	3.6 mg/g

Table 2. Desalination Efficiency of ACC Electrodes and ACC Electrodes Coated with ZnO Nanorods for Different Salt Concentrations[a]

	% Desalination for Different Concentrations of NaCl			
electrode material	2 mM NaCl	17 mM NaCl	50 mM NaCl	100 mM NaCl
ACC	39%	28%	11%	5%
Z_ACC	53%	43%	16%	9%

[a]The experiments were performed in a flat plate symmetric electrode CDI cell having an electrode area of 8.4 cm^2, with an applied potential of 1.6 V and a flow rate of 3 mL/min.

Thus, we can conclude that, with a cut-in voltage of <0.5 V (Figure 5a), at all applied potentials, the electrode surface can be populated with free charges, each of which has its own electric force. These forces contribute to generate a strong adsorption force at the electrode surface all along the length of the rod, penetrating deeper into the electrode gap (Figure 7). This leads to a reduction in the desalination time with a corresponding increase in the desalination efficiency of the electrodes.

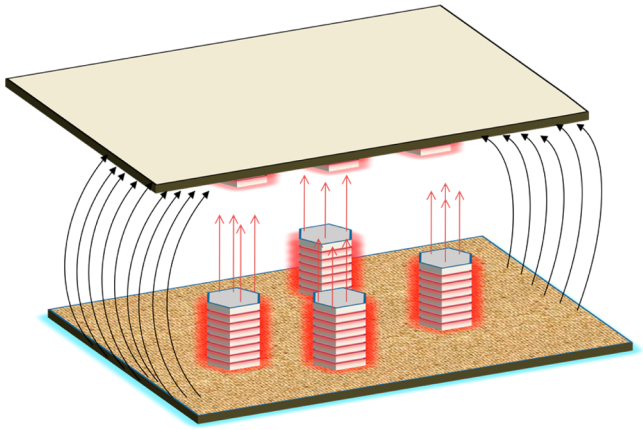

Figure 7. Schematic of electric field distribution on the surface of an ACC electrode coated with ZnO nanorods, showing lines of force distributed uniformly along the surface planes of the rods. Their nonhierarchical structure reduces the shielding effect, compared to ACC, where the hierarchical structure of the pores can reduce the field strength. The black lines indicate the concentration of field lines due to edge effects from the ACC surface, while the red arrows indicate lines of force emanating from the rods.

We also theoretically estimated the total surface utilization of the Z_ACC electrode, with respect to applied potential and desalination efficiency, assuming symmetrical adsorption of Cl^- and Na^+ ions at the positive and negative electrode, respectively (see Section V in the Supporting Information), although it is rarely symmetrical.[30] A plot of surface coverage, with respect to the applied potential and the efficiency of desalination, shows that the CDI cell is oversized, with a majority of the surface being unused (Figure 8). Efforts are presently being made to improve surface utilization and power consumption, with a focus on enhanced field distribution between the electrodes.

The nanorods-coated ACC electrode thus enabled the ions with easy access to the charged surface, leading to an improvement in desalination efficiencies. The improvement was attributed to the electric field present at the ZnO surface, which promotes the fast adsorption process and can be controlled by varying the density and surface coverage of the rods.[25,31] An additional factor that has not been investigated but could be contributing to the increased desalting efficiency could be hydroxylation at the ZnO surface,[32,33] which leads to both cationic and anionic exchange sites,[33,34] leading to improved ion adsorption. Further optimization of ZnO nanorods grown on ACC must be performed to improve electric field distribution, surface utilization, and desalination efficiency.

3. CONCLUSION

By a facile growth of ZnO nanorods on the ACC surface, we were able to improve the electric field distribution between the electrodes, leading to a 22% increase in the charge storage

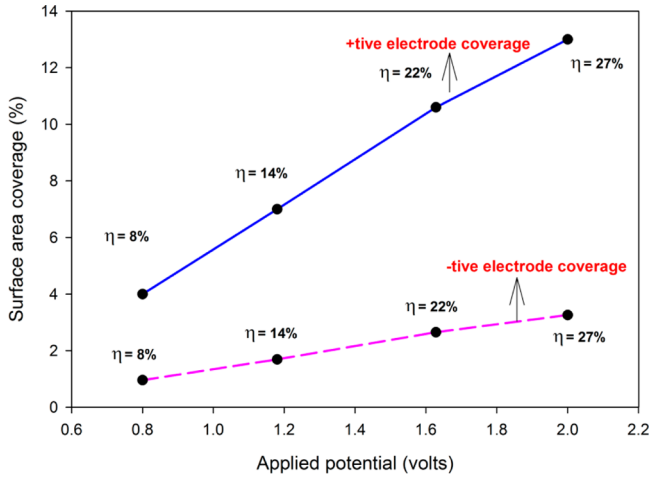

Figure 8. Surface coverage of the positive and negative electrodes with the anions and cations, respectively (assuming symmetric adsorption on either electrode), showing marginal utilization of the Z_ACC surface.

capacity of the electrode, along with faster surface saturation, because of enhancement in the ion adsorption rate. The overall charge efficiency of the device was also improved by 38% at lower applied potentials, leading to an improvement in the desalination efficiency by an average of 45% for applied potentials varying from 0.8 V to 2.0 V. Thus, by growing nanorods, we were able to increase the desalination efficiency, capacitance, and charge efficiency of the electrodes, attributed to a uniform distribution of electric field all along the nanorod surfaces and the easy accessibility of the nanorods for ion adsorption.

4. EXPERIMENTAL SECTION

4.1. Chemicals and Substrates. Analytical-grade zinc acetate dihydrate ($Zn(CH_3COO)_2{\cdot}2H_2O$), sodium hydroxide (NaOH), absolute ethanol (C_2H_5OH), and hydrochloric acid (HCl, 34%) were purchased from Merck, Germany. Zinc nitrate hexahydrate ($Zn(NO_3)_2{\cdot}6H_2O$) was obtained from APS Ajax Finechem, Australia, and hexamethylenetetramine ($(CH_2)_6N_4$) was supplied by Aldrich, USA. All the chemicals were used without any further purification. Activated woven carbon cloth (Zorflex FM-100) was used as substrates for the growth of zinc oxide (ZnO) nanorods that are forming the composite electrodes. Activated carbon cloth (ACC), with a thickness of ca. 1.0 mm and a specific surface area of ~1100 m^2/g,[34,35] was cleaned with highly concentrated 2 M HCl that was heated to 115 °C (slightly above the boiling point of HCl solution) for 12 h to remove mineral contaminants. Subsequently, samples were thoroughly rinsed with deionized water and dried in a vacuum oven at 150 °C for 12 h and then stored in a desiccator until further use.

4.2. Preparation of ZnO Nanoparticles for Seeding Process. ZnO nanoparticle colloid was prepared by following the procedure reported by Baruah et al.[36,37] Briefly, 4 mM NaOH in absolute ethanol was added drop by drop to 4 mM zinc acetate solution (in absolute ethanol) under continuous stirring. The mixture was then hydrolyzed at 60 °C for 2 h for the precipitation of ZnO nanoparticles ca. 6−8 nm in diameter.

Subsequently, clean ACC substrates were dipped in the ZnO colloidal solution for 30 min and dried in an oven at 95 °C for 30 min; this process was repeated twice, and then as-seeded samples were dried in an oven at 95 °C.

4.3. Hydrothermal Growth of ZnO Nanorods. ZnO nanorods were grown on preseeded ACC substrates by a hydrothermal process in an equimolar solution (20 mM) of zinc nitrate hexahydrate and hexamethylenetetramine at 90 °C for a growth time of 10 h.[38] The

precursor solution was replenished every 5 h to ensure an adequate supply of Zn ions for the hydrothermal growth. In order to adjust the initial pH of precursor solution, NaOH solution (pH ~12) was used. Following the hydrothermal growth of ZnO nanorods, the ACC substrates were thoroughly rinsed with deionized water (DI) and annealed at 150 °C for 1 h in air.

4.4. Characterization. The surface morphology of ZnO-coated ACC electrodes were characterized using a field-emission scanning electron microscope (FESEM) system (JEOL, Model JSM-6301F) working at 20 kV. Conductivity measurements were carried out using an online conductivity probe (Model eDAQ_ET916) with a cell volume of 93 μL coupled to a conductivity isopod (Model EPU357) with single-channel PodVu software for real-time recording of the conductivity changes. Cyclic voltammetry measurement were carried out using 0.5 M NaCl solution in an electrochemical cell with a three-electrode system: platinum wire as the counter electrode, Ag/AgCl as the reference electrode, and ACC and ACC coated with ZnO nanorods as working electrodes. This system was controlled using a custom-made potentiostat equipped with NI USB-6009 equipment that was driven by the LabView program. Specific capacitances of the electrodes were calculated by integrating the area under the CV curves, as shown in eq 8:

$$C_s = \int_{E1}^{E2} \frac{I(E)\,dE}{[2(E2 - E1)mv} \tag{8}$$

where C_s is the specific capacitance, $E1$ and $E2$ are the limits of the applied potential, m is the mass of electrode, ν is the scan rate (mV/s), and $i(E)\,dE$ is the power delivered during the scan.

Active surface area measurements were conducted using an NMR relaxation technique in Xigo Nanotools equipment, with water and ethanol as the solvents. In this system, we can probe the spin magnetic moments of hydrogen nuclei in pore fluids to a perturbation in the applied static magnetic field. The perturbation changes the total nuclear magnetization, whose relaxation back to equilibrium can be noted with time (comprising of longitudinal relaxation time T_1, defining the decay of spin alignment and the transverse relaxation time T_2, defining the decay of precession). Here, we extract the T_2 relaxation time of the solvent, which was analyzed by Acorn area software to interpret the surface area of the electrode (using the specific surface relaxivity of activated carbon (κ)) in contact with the solvent. Power consumption was calculated by integrating the charging current decay curve in Matlab to obtain the total charge deposited in one cycle. The charge deposited was multiplied by the applied voltage to get the work done (in joules, J), which was subsequently converted to watts (W). X-ray diffraction measurements of ZnO NR on ACC substrates were carried out by Rigaku Model Miniflex 600 XRD system with a Cu Kα X-ray source (wavelength ≈ 1.54 Å).

4.5. ZnO Current–Voltage (*I*–*V*) Characteristics Measurement. The I–V characteristics of ZnO nanorods were measured by growing ZnO nanorods on a glass substrate using the method described elsewhere.[24] In brief, a ZnO seed layer was deposited on the cleaned substrates by spraying 15 mL of 10 mM zinc acetate [$Zn(CH_3COO)_2{\cdot}2H_2O$] in deionized (DI) water at a rate of 1 mL/min (from a distance of 20 cm) on the cleaned substrates preheated to 420 °C on a hot plate. Seeded substrates were then placed in a chemical bath containing equimolar (20 mM) concentration of zinc nitrate hexahydrate [$Zn(NO_3)_2{\cdot}6H_2O$] and hexamine ($C_6H_{12}N_4$) solution in DI water at 95 °C for 20 h; the solution was replenished every 5 h to form uniform nanorods.[39] The nanorod-coated substrates were then removed from the chemical bath, rinsed thoroughly with DI water, and annealed in air at 350 °C for 60 min. The annealed samples were masked in the center, while gold was sputtered at the edges (with an electrode gap of 5 mm) to form a Schottky contact with ZnO. A drop of mercury was then placed on the tip of the nanorods (serving as one electrode), while gold deposited at the edges served as the counter electrode. A Keithley Model 617 programmable electrometer was used as an input voltage source and a current meter, to measure the output current and record the I–V characteristics of the devices.

4.6. Capacitive Deionization Experiments. The desalination/regeneration experiments were conducted using flow-through capacitor model. The CDI cell consists of symmetrical electrodes of 8.41 cm^2, a spacer with a thickness of ca. 650 μm, a reservoir composed of poly(methyl methacrylate) (PMMA) (Dow Corning SYLGARD 184 silicone elastomer kit), a current collector (graphite electrode), and an acrylic plate to organize the CDI cell (see Figure S1 in the Supporting Information). The current collectors were used as electrical connection from power supply (DC) to the ACC:ZnO electrodes.

In order to perform the complete cycle of ion removal from the saline solution, ion adsorption during desalination and desorption during regeneration (refreshment of the electrodes in CDI cell was necessary prior to the next step of desalination) were recorded. This process was carried out using 1000 ppm sodium chloride (NaCl) solution with a flow rate of 3 mL/min under variable applied potentials ranging from 0.8 V to 2.0 V. A peristaltic pump (Heidolph Model 5201 pump drive) was used to maintain a constant flow rate of the saline water into the CDI cell. The total charging (desalination) time was based on electrode saturation; i.e., when the conductivity of the outlet solution stopped decreasing and started increasing. Similarly, the discharging (regeneration) time was considered to be the time taken by the flushing solution (under short-circuit conditions) to reach the initial conductivity. A test bench comprising a power supply, a data logging system, and pH and conductivity measurements was assembled to measure the variables involved for characterization of the CDI cells (Figure S1 in the Supporting Information).

Charge efficiency (η) was calculated as the ratio of electrosorption capacity of electrodes in terms of charge (Λ) to the total amount of charge delivered during the adsorption cycle (Q_t), as shown in eq 9:[40]

$$\Lambda = \frac{(\Delta_\sigma M_w V)F}{mc} \tag{9}$$

where Δ_σ is the gradient in conductivity between desalination and regeneration, M_w the molar mass of NaCl, V the volume of solution, m the mass of electrode, F the Faraday constant (F = 96 485.3365 C/mol), and c the slope of conductivity, with respect to salt concentration.

■ ASSOCIATED CONTENT

Ⓢ Supporting Information

Supporting information for the manuscript contains information and data on CDI cell construction scheme, XRD diffractograms of ZnO nanorods grown on the ACC surface, cyclic voltammaograms of the composite ACC_ZnO and plain ACC electrodes, NMR-based active surface area measurements on plain ACC and ZnO_ACC, electrode surface area utilization calculation, and desalination repeatability curves for the applied potentials. This material is available free of charge via the Internet at http://pubs.acs.org.

■ AUTHOR INFORMATION

Corresponding Author

*E-mail: dutta@squ.edu.om.

Notes

The authors declare no competing financial interest.

■ ACKNOWLEDGMENTS

The authors would like to thank the Chair in Nanotechnology, The Research Council of Oman (TRC) and Sultan Qaboos University for financial support.

■ REFERENCES

(1) Shiklomanov, I. A. Appraisal and Assessment of World Water Resources. *Water Int.* **2000**, *25*, 11–32.

(2) Zhao, R.; Porada, S.; Biesheuvel, P. M.; van der Wal, A. Energy Consumption in Membrane Capacitive Deionization for Different Water Recoveries and Flow Rates, and Comparison with Reverse Osmosis. *Desalination* **2013**, *330*, 35−41.
(3) Cohen, I.; Avraham, E.; Soffer, A.; Aurbach, D. Water Desalination by Capacitive Deionization—Advantages Limitations and Modification. *ECS Trans.* **2013**, *45*, 43−59.
(4) Biesheuvel, P. M.; van Limpt, B.; van der Wal, A. Dynamic Adsorption/Desorption Process Model for Capacitive Deionization. *J. Phys. Chem. C* **2009**, *113*, 5636−5640.
(5) Porada, S.; Zhao, R.; van der Wal, A.; Presser, V.; Biesheuvel, P. M. Review on the Science and Technology of Water Desalination by Capacitive Deionization. *Prog. Mater. Sci.* **2013**, *58*, 1388−1442.
(6) García-Quismondo, E.; Santos, C.; Lado, J.; Palma, J.; Anderson, M. A. Optimizing the Energy Efficiency of Capacitive Deionization Reactors Working under Real-World Conditions. *Environ. Sci. Technol.* **2013**, *47*, 11866−11872.
(7) Huang, W.; Zhang, Y.; Bao, S.; Song, S. Desalination by Capacitive Deionization with Carbon-Based Materials as Electrode: A Review. *Surf. Rev. Lett.* **2013**, *20*.
(8) Oh, H.-J.; Lee, J.-H.; Ahn, H.-J.; Jeong, Y.; Kim, Y.-J.; Chi, C.-S. Nanoporous Activated Carbon Cloth for Capacitive Deionization of Aqueous Solution. *Thin Solid Films* **2006**, *515*, 220−225.
(9) Ryoo, M.-W.; Kim, J.-H.; Seo, G. Role of Titania Incorporated on Activated Carbon Cloth for Capacitive Deionization of NaCl Solution. *J. Colloid Interface Sci.* **2003**, *264*, 414−419.
(10) Lanje, A. S.; Sharma, S. J.; Ningthoujam, R. S.; Ahn, J. S.; Pode, R. B. Low Temperature Dielectric Studies of Zinc Oxide (ZnO) Nanoparticles Prepared by Precipitation Method. *Adv. Powder Technol.* **2013**, *24*, 331−335.
(11) Salim, N. T.; Aw, K. C.; Gao, W.; Li, Z. W.; Wright, B. ZnO as a Dielectric for Organic Thin Film Transistor-Based Non-Volatile Memory. *Microelectron. Eng.* **2009**, *86*, 2127−2131.
(12) Ryoo, M.-W.; Seo, G. Improvement in Capacitive Deionization Function of Activated Carbon Cloth by Titania Modification. *Water Res.* **2003**, *37*, 1527−1534.
(13) Ling, T.; Song, J.-G.; Chen, X.-Y.; Yang, J.; Qiao, S.-Z.; Du, X.-W. Comparison of ZnO and TiO_2 Nanowires for Photoanode of Dye-Sensitized Solar Cells. *J. Alloys Compd.* **2013**, *546*, 307−313.
(14) Cheng, B.; Samulski, E. T. Hydrothermal Synthesis of One-Dimensional ZnO Nanostructures with Different Aspect Ratios. *Chem. Commun.* **2004**, 986−987.
(15) Baruah, S.; Dutta, J. Hydrothermal Growth of ZnO Nanostructures. *Sci. Technol. Adv. Mater.* **2009**, *10*.
(16) Myint, M. T. Z.; Dutta, J. Fabrication of Zinc Oxide Nanorods Modified Activated Carbon Cloth Electrode for Desalination of Brackish Water Using Capacitive Deionization Approach. *Desalination* **2012**, *305*, 24−30.
(17) Baruah, S.; Thanachayanont, C.; Dutta, J. Growth of ZnO Nanowires on Nonwoven Polyethylene Fibers. *Sci. Technol. Adv. Mater.* **2008**, *9*, 025009.
(18) Baruah, S.; Jaisai, M.; Imani, R.; Nazhad, M. M.; Dutta, J. Photocatalytic Paper Using Zinc Oxide Nanorods. *Sci. Technol. Adv. Mater.* **2010**, *11*, 055002.
(19) Jo, S. H.; Banerjee, D.; Ren, Z. F. Field Emission of Zinc Oxide Nanowires Grown on Carbon Cloth. *Appl. Phys. Lett.* **2004**, *85*, 1407−1409.
(20) Xu, C. X.; Sun, X. W. Field Emission from Zinc Oxide Nanopins. *Appl. Phys. Lett.* **2003**, *83*, 3806−3808.
(21) Yu, K.; Zhang, Y. S.; Xu, F.; Li, Q.; Zhu, Z. Q.; Wan, Q. Significant Improvement of Field Emission by Depositing Zinc Oxide Nanostructures on Screen-Printed Carbon Nanotube Films. *Appl. Phys. Lett.* **2006**, *88*, -.
(22) Yan, C.; Zou, L.; Short, R. Polyaniline-Modified Activated Carbon Electrodes for Capacitive Deionisation. *Desalination* **2014**, *333*, 101−106.
(23) Daley, M. A.; Tandon, D.; Economy, J.; Hippo, E. J. Elucidating the Porous Structure of Activated Carbon Fibers Using Direct and Indirect Methods. *Carbon* **1996**, *34*, 1191−1200.
(24) Sugunan, A.; Warad, H.; Boman, M.; Dutta, J. Zinc Oxide Nanowires in Chemical Bath on Seeded Substrates: Role of Hexamine. *J. Sol−Gel Sci. Technol.* **2006**, *39*, 49−56.
(25) Pan, N.; Xue, H.; Yu, M.; Cui, X.; Wang, X.; Hou, J. G.; Huang, J.; Deng, S. Z. Tip-Morphology-Dependent Field Emission from ZnO Nanorod Arrays. *Nanotechnology* **2010**, *21*.
(26) Tseng, Y. K.; Huang, C. J.; Cheng, H. M.; Lin, I. N.; Liu, K. S.; Chen, I. C. Characterization and Field-Emission Properties of Needle-Like Zinc Oxide Nanowires Grown Vertically on Conductive Zinc Oxide Films. *Adv. Funct. Mater.* **2003**, *13*, 811−814.
(27) Bora, T.; Kyaw, H. H.; Sarkar, S.; Pal, S. K.; Dutta, J. Highly Efficient ZnO/Au Schottky Barrier Dye-Sensitized Solar Cells: Role of Gold Nanoparticles on the Charge-Transfer Process. *Beilstein J. Nanotechnol.* **2011**, *2*, 681.
(28) Zhao, Y.; Wang, Y.; Wang, R.; Wu, Y.; Xu, S.; Wang, J. Performance Comparison and Energy Consumption Analysis of Capacitive Deionization and Membrane Capacitive Deionization Processes. *Desalination* **2013**, *324*, 127−133.
(29) Anderson, M. A.; Cudero, A. L.; Palma, J. Capacitive Deionization as an Electrochemical Means of Saving Energy and Delivering Clean Water. Comparison to Present Desalination Practices: Will It Compete? *Electrochim. Acta* **2010**, *55*, 3845−3856.
(30) Gao, X.; Landon, J.; Neathery, J. K.; Liu, K. Modification of Carbon Xerogel Electrodes for More Efficient Asymmetric Capacitive Deionization. *J. Electrochem. Soc.* **2013**, *160*, E106−E112.
(31) Jo, S. H.; Lao, J. Y.; Ren, Z. F.; Farrer, R. A.; Baldacchini, T.; Fourkas, J. T. Field-Emission Studies on Thin Films of Zinc Oxide Nanowires. *Appl. Phys. Lett.* **2003**, *83*, 4821−4823.
(32) Noei, H.; Qiu, H.; Wang, Y.; Loffler, E.; Woll, C.; Muhler, M. The Identification of Hydroxyl Groups on ZnO Nanoparticles by Infrared Spectroscopy. *Phys. Chem. Chem. Phys.* **2008**, *10*, 7092−7097.
(33) Tamura, H.; Mita, K.; Tanaka, A.; Ito, M. Mechanism of Hydroxylation of Metal Oxide Surfaces. *J. Colloid Interface Sci.* **2001**, *243*, 202−207.
(34) Shim, J. W.; Park, S. J.; Ryu, S. K. Effect of Modification with HNO_3 and NaOH on Metal Adsorption by Pitch-Based Activated Carbon Fibers. *Carbon* **2001**, *39*, 1635−1642.
(35) Brasquet, C.; Le Cloirec, P. Effects of Activated Carbon Cloth Surface on Organic Adsorption in Aqueous Solutions. Use of Statistical Methods to Describe Mechanisms. *Langmuir* **1999**, *15*, 5906−5912.
(36) Makhal, A.; Sarkar, S.; Bora, T.; Baruah, S.; Dutta, J.; Raychaudhuri, A. K.; Pal, S. K. Dynamics of Light Harvesting in ZnO Nanoparticles. *Nanotechnology* **2011**, *21*, 265703−265707.
(37) Baruah, S.; Rafique, R. F.; Dutta, J. Visible Light Photocatalysis by Tailoring Crystal Defects in Zinc Oxide Nanostructures. *Nano* **2008**, *03*, 399−407.
(38) Baruah, S.; Dutta, J. Effect of Seeded Substrates on Hydrothermally Grown ZnO Nanorods. *J. Sol−Gel Sci. Technol.* **2009**, *50*, 456−464.
(39) Baruah, S.; Dutta, J. pH-Dependent Growth of Zinc Oxide Nanorods. *J. Cryst. Growth* **2009**, *311*, 2549−2554.
(40) Gao, X.; Omosebi, A.; Landon, J.; Liu, K. Enhancement of Charge Efficiency for a Capacitive Deionization Cell Using Carbon Xerogel with Modified Potential of Zero Charge. *Electrochem. Commun.* **2014**, *39*, 22−25.